Journal of Non-Crystalline Solids 373–374 (2013) 51–56

Contents lists available at SciVerse ScienceDirect

Journal of Non-Crystalline Solids

journal homepage: www.elsevier.com/ locate/ jnoncrysol

Ab initio and Raman study of medium range ordering in $GeSe_2$ glass

R. Holomb [a,*], V. Mitsa [a], E. Akalin [b], S. Akyuz [c], M. Sichka [a]

[a] Institute of Solid State Physics and Chemistry, Uzhhorod National University, 88000 Uzhhorod, Ukraine
[b] Istanbul University, Physics Department, Science Faculty, 34134 Istanbul, Turkey
[c] Istanbul Kultur University, Physics Department, Faculty of Science and Letters, 34156 Istanbul, Turkey

ARTICLE INFO

Article history:
Received 13 February 2013
Received in revised form 10 April 2013
Available online xxxx

Keywords:
Ab initio;
DFT;
Finite nanoclusters;
$GeSe_2$ glass;
Raman spectra

ABSTRACT

High resolution Raman spectra of $GeSe_2$ glass were measured and fitted using individual Gaussian components. The structural origin of the components were interpreted using the results of *ab initio* density functional theory calculations performed on Ge_nSe_m nanoclusters (n = 2–6, 12; m = 6–9, 12, 14–16, 30) which represent the local structure of $GeSe_2$ glass and on some "defect" Ge_nSe_m clusters that are thought to be related to the inhomogeneity of the structure at the nanoscale. The calculated vibrational properties of Ge_nSe_m nanoclusters and their couplings with the short- and medium-range order structure formations in $GeSe_2$ glass are analyzed and discussed.

1. Introduction

Amorphous chalcogenides in their glass and thin film forms are attractive class of non-crystalline semiconductor materials [1,2]. Due to the unique physico-chemical properties of Ge-based chalcogenides they have a wide range of applications in infrared (IR) and non-linear optics, photonics, ultrafast signal processing and optical regeneration, information recording, biosensing *etc.* [3–17]. The stoichiometric $GeSe_2$ glass (hereafter denoted as *g*-$GeSe_2$) composition has been the subject of great scientific and technological interest since it is a promising material for IR optical and non-linear photonics applications [9,18–23]. In addition, *g*-$GeSe_2$ shows various kinds of light-induced structural changes in processes such as photo-bleaching, photo-crystallization, and photo-induced diffusion [24,25]. The photo modification properties of dichalcogenides can be applied to the branch couplers, interferometers, waveguides, nano-lens and photo-resist materials for the micro- and nano-fabrication. Also, $GeSe_2$ is a "canonical" model object of the binary Ge–Se glass system with the complex structure, particularly in view of achieving a description of the relationship between the short- and medium-range ordering, local dimensionality and structural transition at the atomic scale and the resulting electronic and optical properties [26,27].

It is well known that crystalline $GeSe_2$ exists in two different modifications; low-temperature (LT or α) and high-temperature (HT or β) [28–32]. The synthesis of additional high temperature form of $GeSe_2$ (γ-$GeSe_2$) was reported in [33]. The common structural motif of α- and β-$GeSe_2$ is a 6-member ring consisting three sharing GeS_4 tetrahedra. The 3D network of LT $GeSe_2$ phase represents mutually connected 6-member rings. In contrast with LT, the HT-$GeSe_2$ also contains 4-member rings or so called edge-sharing $GeSe_4$ tetrahedra. The layer-like 2D network of HT-$GeSe_2$ can be viewed as infinite parallel chains of 6-member rings connected by edge-sharing (4-member ring) blocks. The structure (especially at medium range order (MRO) scale) of a glassy state of $GeSe_2$ is more complex since it contains homopolar Ge–Ge and Se–Se bonds and has been the subject of extensive studies during the last decade [27,34–40].

Recently we have performed *ab initio* density functional theory (DFT) calculations on Ge_nSe_m nanoclusters that represent the local structure of $GeSe_2$ glass and on some "defect" Ge_nSe_m clusters that are thought to be related to the inhomogeneity of the structure at the nanoscale [41]. In this work we present the results of *ab initio* calculations together with Raman studies of binary $GeSe_2$ glass. The detailed analysis of total cluster energies and their derivatives shows the preference in formation of four- and six-member rings and bigger clusters that are topologically similar to the β-$GeSe_2$. We have found that the formations of so called "wrong" Ge–Ge and Se–Se bonds are energetically favorable when they are incorporated in five-member rings rather than in form of ethane-like cluster with Ge–Ge bond and cluster with Se–Se bridge. Also, some peculiarities in electronic properties of clusters with Se–Se bonds and their correlations with dihedral and bond angles were established [41]. We report here the results of extended spectroscopic studies on Ge_nSe_m nanoclusters in order to elucidate the medium range structures of *g*-$GeSe_2$. The calculated frequencies (~219 cm^{-1} (i = 4), ~203 cm^{-1} (i = 6) and ~191–194 cm^{-1} (i = 8,10)) of main Raman active modes of Ge–Se stretching vibrations of *i*-member rings demonstrate red-shifting with increasing ring size (i). Also, the Raman mode at ~176 cm^{-1} was calculated for

* Corresponding author. Tel.: +380 31 22 33020; fax: +380 31 22 32339.
E-mail address: holomb@ukr.net (R. Holomb).

0022-3093/$ – see front matter © 2013 Elsevier B.V. All rights reserved.
http://dx.doi.org/10.1016/j.jnoncrysol.2013.04.032

5-member ring with "wrong" Ge – Ge bond. The contribution of calculated Raman active modes of 4-, 5-, 6-, 8-, 10-member rings and bigger Ge_nSe_m nanoclusters in the curve fitted micro-Raman and FT-Raman spectra of $GeSe_2$ glass is analyzed and discussed in detail.

2. Experimental and theoretical details

2.1. Sample preparation and experimental details

The bulk germanium diselenide glasses were prepared by the conventional melt-quenching route from a mixture of high purity 99.999% Ge and Se precursors in evacuated and sealed quartz ampoules placed in a rocking furnace to obtain the most homogeneous melt. First the ampoules were heated with the rate of 2–3 K/min and kept at 873–900 K for 18–20 h. Then with the rate of 1–2 K/min the temperature was increased above the liquidus temperature (1013 K) and was kept constant at 1070 K during 20–30 h. All ingots were quenched by switching off the furnace and cooled in ice water (275–277 K). The additional details can also be found in [42,43].

High resolution FT-Raman spectra of $GeSe_2$ glasses were measured using a Bruker MULTIRAM FT-Raman spectrometer. Near-IR Nd:YAG laser with a wavelength of 1064 nm ($E_{ex.1} = 1.17$ eV) was used as excitation source. A Jasco NRS 3100 Raman spectrometer equipped with CCD detector was used for recording the micro-Raman spectra (1200 lines/mm grating) with a diode laser operating at 785 nm ($E_{ex.2} = 1.58$ eV) as the excitation source. All measurements were performed at room temperature in back-scattering geometry. To obtain the high signal-to-noise ratio, 200 spectra were accumulated and spectral resolution was 2 cm^{-1}. To yield peak positions and intensity values, the experimental Raman spectra were fitted using Gaussian type functions with prior subtraction of a background and fitting was undertaken until reproducible and converged results were obtained with squared correlations better than $r^2 \sim 0.99998$. GRAMS/AI 7.02 (Thermo Electron Corporation) software package was used for spectral manipulations. During the band fitting procedure the full-width-at-half-maximum (FWHM) was held free for all individual components. The position and the intensity of the peaks were allowed to vary freely and independently of each other. The second derivative profile gives valuable information about the position of the bands and band widths. Thus for the band fitting procedure (to locate the position of the peaks), the second derivative profiles of the absorption spectra obtained by using Savitzky–Golay function (second degree polynomial, 17 points) were used as a guide.

2.2. Modeling and calculations

The first stage of our modeling of the local amorphous structures is based on the structure of corresponding crystals. The $GeSe_4$ tetrahedron in the structure of LT α-form of $GeSe_2$ is mutually connected by their corners and forms the three-dimensional (3D) crystal network [28,29]. However HT β-form generates two-dimensional (2D) network built-up by combination of $GeSe_4$ tetrahedra with corner- and edge-sharing geometries [30–32]. In this network the parallel endless chains of corner-sharing tetrahedra are linked together by edge-sharing tetrahedra (Fig. 1). Thus, the short range order (SRO) structure representing α-$GeSe_2$ is corner-sharing tetrahedra and the SRO structures representing β-form of $GeSe_2$ crystal are corner- and edge-sharing tetrahedra (models I and II). The larger cluster which can be found in the crystal structure of $GeSe_2$ is a six-member ring consisting three $GeSe_4$ tetrahedra connected by their corners (III). It should be noted here that two edge-sharing tetrahedra can also be classified as four-member ring. Models IV and V represent two six-member rings selected from two directions of 2D network of β-$GeSe_2$ crystal. In the first case the rings are connected by common Ge while in the other model rings are connected *via* the edge-sharing block. The largest cluster obtained from the crystal structure of $GeSe_2$ monolayer (VI) consists of a big 16-member ring.

It is well known that the structure of amorphous state is very sensitive to the synthesis condition and production technology [26,44]. The significant difference between amorphous and crystalline states in the structure and in the properties could be due to the formation of "defects" which include either homopolar (or so called "wrong") bonds in binary systems or a non-typical chemical coordination and non-typical geometry in comparison to the crystals of corresponding compositions. The *ab initio* methods are very useful to analyze different possible "defect" configurations. Here we represent few possible models with homopolar Ge – Ge (VII–VIII) and Se – Se (IX–XI) bonds. The simplest model of Ge – Ge bond can be seen in the hypothetical cluster, so called ethane-like geometry (VII) [45]. In a similar way homopolar Se – Se bond can be realized as a linkage between two $GeSe_4$ tetrahedra (IX). There is also a possibility of Se – Se bond formation on the edge of the so-called outrigger raft structure (model XI represents the part of this structure) [46]. Recent investigation of the structure of Ge_4Se_9 crystal shows that there is another possibility to form Se – Se bond through $Ge_2Se_{3+4/2}$ cluster (X) which substitutes edge-sharing blocks in 2D crystalline network of β-$GeSe_2$ [47,48]. This cluster together with the model VIII represents five-member rings with incorporated Se – Se and Ge – Ge bonds, respectively. *Ab initio* molecular dynamics (MD) simulations show that in addition to six- and four-member rings the other types of *i*-member rings (i = 3–12) in the structure of liquid and glassy $GeSe_2$ can be seen [37–40]. Therefore in the present study we extend our analysis to larger *i*-member rings (XII and XIII). According to X-ray photoelectron spectroscopy studies performed by Sanghera and co-workers the concentration of non-bridging bonds of selenium atoms in the stoichiometric $GeSe_2$ and As_2Se_3 glass compositions is negligibly small [49,50]. Therefore we did not consider these cluster models with non-bridging chalcogens. It should be noted, however, that similar to silicate glasses the addition of "network modifiers" such as alkali selenides to $GeSe_2$ glass can produce non-bridging atoms [49,51].

The dangling bonds of the surface atoms of the selected finite Ge_nSe_m models were saturated by hydrogen atoms for a better representation of the cluster boundaries and H-terminated Ge_nSe_m nanoclusters used for further *ab initio* calculations. The computational part consists of *ab initio* DFT calculations performed using the Gaussian-03 quantum-chemical program package [52]. The self-consistent DFT field method [53] was applied for geometry optimizations of the clusters using the Berny optimization procedure. The LANL2DZdp ECP basis set of Hay and Wadt [54] with polarization function [55] was used for the Ge, Se and H atoms together with the full Heyd–Scuseria–Ernzerhof hybrid functional based on a screened Coulomb potential (HSE06) [56,57]. Subsequent second derivative calculations verified the obtained structures as true energy minimum geometries. The determined second derivatives of the potential energies of optimized structures were then used to calculate the harmonic vibrational frequencies. To obtain the Raman activities of the clusters it is necessary to determine the mean and anisotropy of the polarizability derivative tensors. The electric dipole moment derivative method implemented in Gaussian-03 software was used to produce the Raman activities of the vibrational modes of Ge–Se clusters. The polarizability derivatives were obtained by numerical differentiation of calculated dipole moment derivatives with respect to the electrical field. The influence of the hydrogen atoms in the calculated Raman spectra of Ge_nSe_m clusters was eliminated using the algorithm described in [58].

3. Results and discussion

3.1. Experimental Raman spectra of $GeSe_2$ glass

In general, the vibrational spectra of $GeSe_2$ glass can be interpreted using the idealized structural model which contains tetrahedrally

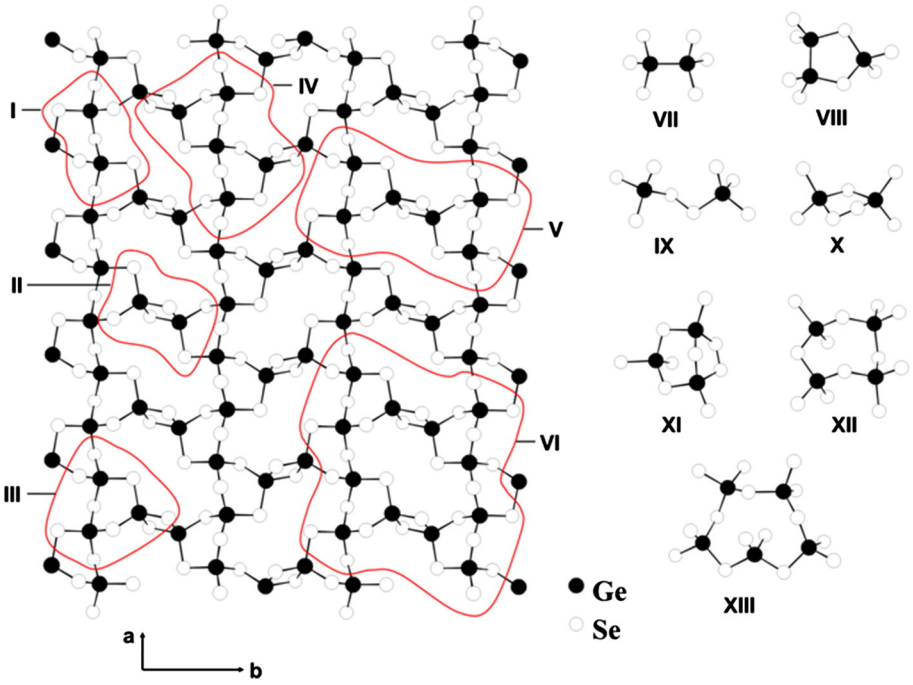

Fig. 1. The crystal structure of high temperature (β) $GeSe_2$ monolayer [32] with the selected Ge_nSe_m cluster models (I–VI) (left) and the "defect" Ge_nSe_m cluster geometries with homopolar Ge – Ge (VII–VIII) and Se – Se (IX–XI) bonds together with the larger eight- and ten-member rings (right). Saturating hydrogen atoms and corresponding bonds are not shown for clarity.

coordinated Ge atoms and twofold coordinated Se atoms. The dominant Raman active mode at ~200 cm^{-1} may be assigned to the full symmetric Ge – Se stretching vibration of the essentially decoupled $GeSe_4$ tetrahedron and to the symmetric stretching vibrations of bridging Se atoms of corner-sharing tetrahedra [59–62]. The so called "companion" line of the dominant Raman mode at ~220 cm^{-1} may involve the contribution from Ge_6Se_6 rings [63]. The structural origin of this mode is still debated. It may be connected either with the breathing vibrations of Se atoms of edge-sharing $GeSe_4$ configuration [60] or with the contribution from structures with Ge – Ge bonds resulting from nanoscale separation [64,65]. The later is also supported by the presence in the Raman spectra of $GeSe_2$ glass of a mode at ~180 cm^{-1} which originate from Ge – Ge stretching vibrations of ethane-like units [66]. Fig. 2 shows the measured micro-Raman ($E_{ex.1}$ = 1.58 eV) and FT-Raman ($E_{ex.2}$ = 1.17 eV) spectra of *g*-$GeSe_2$. As can be seen the spectra demonstrate differences only in the low frequency spectral region (<150 cm^{-1}) caused by the notch filters used to reject elastically scattered light. These two spectra in the 150–350 cm^{-1} region show

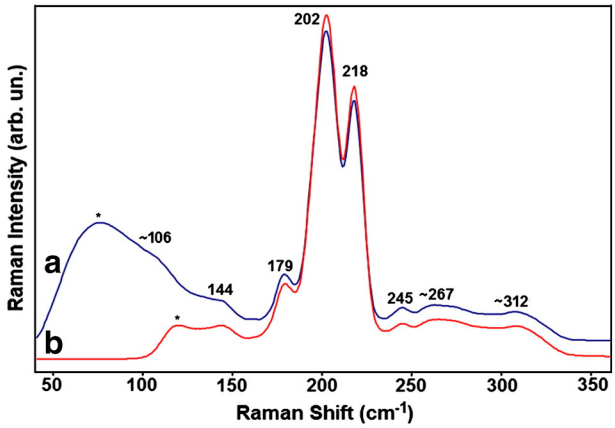

Fig. 2. FT-Raman (1064 nm excitation) (a) and micro-Raman (785 nm excitation) (b) spectra of $GeSe_2$ glass.

no structural changes that indicate quasi-crystallization as observed in [67–69]. In addition to two main bands at 202 and 218 cm^{-1}, bands at 179 and 245 cm^{-1} and two complex broad bands centered at ~267 and ~312 cm^{-1} were detected. The 202 and 218 cm^{-1} Raman modes are related with the Ge – Se stretching vibrations in so called corner- and edge-sharing tetrahedra, respectively [70–72]. However, the former mode can also be a characteristic vibration of outrigger raft cluster [46]. The bands at 179 and 245 cm^{-1} may be connected with stretching Ge – Ge vibrations of ethane like cluster and Se – Se stretching vibrations, respectively [72,73].

Our recent theoretical study on formation energy, stability and electronic properties of different Ge_nSe_m clusters indicates that the formation of single ethane like cluster, single corner sharing $GeSe_4$ tetrahedra and cluster based on two $GeSe_4$ tetrahedra connected by Se – Se bridge was energetically not favorable structural motifs [41]. On the other hand we have found that the ring-like structures were most favorable within our Ge_nSe_m cluster models. In one of our previous studies [44] we have found that the vibrational mode at ~250 cm^{-1} observed in the Raman spectra of GeS_2 glass can be interpreted as the existence of GeS microphase rather than ethane-like Ge_nS_m cluster with Ge – Ge bond.

3.2. Calculated Raman spectra of Ge–Se cluster models

The calculated Raman spectra of Ge_nSe_m nanoclusters are shown in Fig. 3. As can be seen from Fig. 3A the main experimental Raman modes observed at 179, 202 and 218 cm^{-1} (see Fig. 2) can be described very well using small Ge_nSe_m clusters (SRO regime). The Ge – Ge stretching vibration in ethane-like cluster was calculated at 176 cm^{-1}. The Ge – Se stretching vibrations were calculated at 202 and 219 cm^{-1} for corner- and edge-sharing tetrahedra, respectively. The calculated Se – Se vibration in model IX was found at 287 cm^{-1} which is slightly higher than expected. Later we will analyze and discuss whether the high energy shift of Se – Se stretching vibration is connected to the method used for calculation or not. The small gas phase nanoclusters have deformational vibrations below 150 cm^{-1}

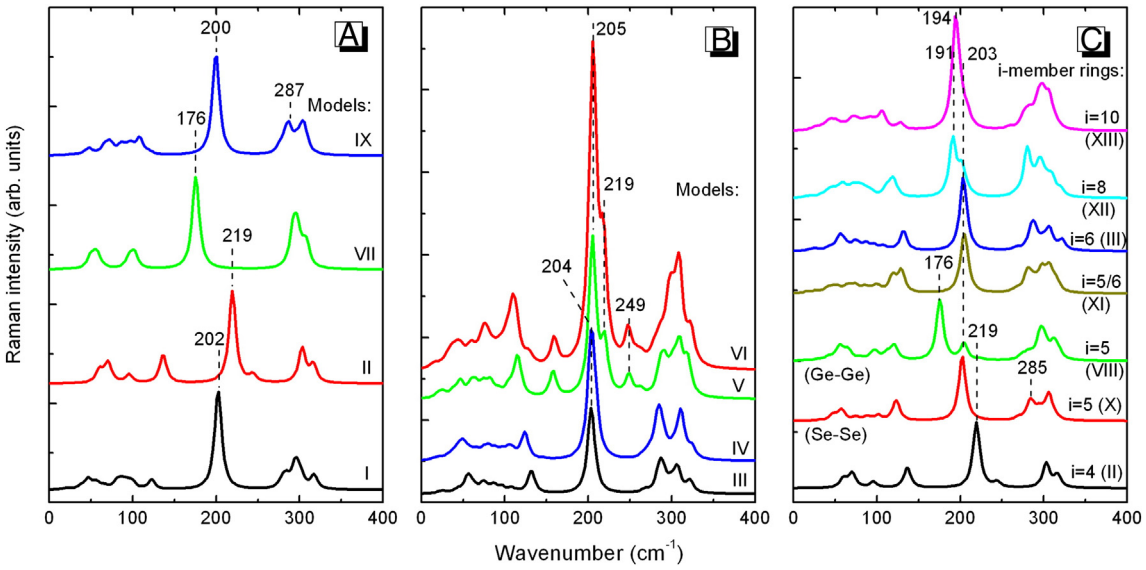

Fig. 3. Simulated Raman spectra of Ge_nSe_m clusters calculated at HSE06/LANL2DZ ECP polarized (p,d) level of theory: spectra of Ge_nSe_m clusters at SRO regime (A), evolution of spectra of Ge_nSe_m clusters topologically similar with HT-$GeSe_2$ (B), and spectra of *i*-member ring Ge_nSe_m clusters (C).

and vibrational modes around 300 cm^{-1} that originate from IR active asymmetric Ge – Se stretching vibrations.

With increasing cluster size (Fig. 3B) an additional Raman active mode was found at ~250 cm^{-1}. Also, we have observed low energy shift of the Ge – Se stretching vibrations from ~203 to 194/191 cm^{-1} with increasing ring size from $i = 6$ to $i = 8/10$ (Fig. 3C). The main calculated mode frequencies of Ge – Se, Ge – Ge and Se – Se stretching vibrations of Ge_nSe_m clusters, their Raman activities and assignments are tabulated in Table 1.

Observed peculiarities in the calculated Raman spectra of our Ge–Se cluster models were used to distinguish the different MRO structures in the $GeSe_2$ glass structure. For this purpose we have performed curve fitting procedure on high resolution Raman spectra of *g*-$GeSe_2$ using independent Gauss functions. The result of curve fitting is summarized in Fig. 4. As clearly seen the main vibrational mode centered at ~202 cm^{-1} in the Raman spectra of *g*-$GeSe_2$ consists of two peaks located at 204.1 and 195.9 cm^{-1}. The former is in very good accordance with the Raman mode at 204/205 cm^{-1} calculated for six-member rings and larger ring-like Ge_nSe_m clusters topologically similar with HT-$GeSe_2$ (Fig. 3B). We suppose that the mode at 195.9 cm^{-1} originates from larger rings with $i = 8$, 10 (Fig. 3C). The additional signature for the existence of big clusters topologically similar with HT-$GeSe_2$ is the band at 243.7 cm^{-1} observed in the curve fitted Raman spectra of *g*-$GeSe_2$. Such mode is calculated at 248.8 and 247.4 cm^{-1} for models V and VI, respectively (See Fig. 3B and Table 1). Thus, it is possible to distinguish between four-, six- and larger (eight-, ten-) member Ge–Se rings in the structure of *g*-$GeSe_2$: the four- and six-member rings occur in the structure of $GeSe_2$ glass with nearly the same concentration while the concentration of larger eight- and ten- member rings is less but quite significant.

It is not possible to find evidence of an energetically more favorable model of five-member rings describing homopolar Ge – Ge and Se – Se bonds [41] using Raman spectroscopy. The calculated Ge – Ge vibration yields the same frequency (175.5 cm^{-1}) for both ethane-like and five-member ring models (Table 1). Also, the Se – Se stretching vibrations within our Ge – Se clusters calculated at 287.2, 283.3 and 284.5 cm^{-1} for models IX, X and XI, respectively cannot be distinguished due to broadening and overlapping of asymmetric Ge – Se stretching vibrations.

To analyze the frequency position of the Se – Se stretching vibrations in Ge_nSe_m clusters (models IX–XI) we have calculated Raman spectra of Se_n ($n = 12$) chain (helical Se) and Se_8 ring using the same method and basis set and compared it with the experimental FT-Raman spectrum of amorphous Se (*a*-Se) (Fig. 5). The main bands of Se – Se stretching vibrations of helical Se and Se_8 ring were calculated at 265 and 271 cm^{-1}, respectively. This is slightly higher than the main Raman band at 250 cm^{-1} observed in the experimental Raman spectra of *a*-Se. However, the calculated Raman modes at 265 and 271 cm^{-1} are in good accordance with the observed bands at 259 and 268 cm^{-1} which are characteristic Se – Se symmetric bond stretching of Se chain and Se_8 ring respectively of selenium species confined in zeolite matrix [74,75]. Therefore the differences between the frequency positions of Se – Se stretching vibrations of calculated Raman spectra of isolated Se_n chain and Se_8 ring, and the experimental Raman spectra of *a*-Se are mainly due to the intermolecular interaction in the bulk solid.

Table 1
Characteristic Raman active modes of Ge – Se, Ge – Ge and Se – Se stretching vibrations calculated for Ge_nSe_m nanoclusters (DFT/HSE06/LANL2DZ ECP polarized (p,d)).

Model	Frequencies, (cm^{-1})	Raman activities, (Å^4/a.m.u.)	Assignment
I	202.2	42.1	ν_{sym}(Ge – Se)
II	219.3	39.1	ν_{sym}(Ge – Se) (4-mem. ring) (in phase)
	243.8	3.1	ν_{sym}(Ge – Se) (4-mem. ring) (out of phase)
III	203.4	42.6	ν_{sym}(Ge – Se)
IV	203.9	41.2	ν_{sym}(Ge – Se)
	205.0	78.2	ν(Ge – Se) (6-mem. ring)
V	219.5	25.3	ν_{sym}(Ge – Se) (4-mem. ring) (in phase)
	248.8	10.8	ν_{sym}(Ge – Se) (4-mem. ring) (out of phase)
VI	206.4	85.3	ν_{sym}(Ge – Se) (6-mem. ring)
	218.3	35.0	ν_{sym}(Ge – Se) (4-mem. ring) (in phase)
	247.4	9.8	ν_{sym}(Ge – Se) (4-mem. ring) (out of phase)
VII	175.5	39.7	ν(Ge – Ge)
	292.0	12.7	ν(Ge – Se)
VIII	175.5	36.5	ν(Ge – Ge)
	204.3	10.0	ν_{sym}(Ge – Se)
IX	199.5	38.2	ν_{sym}(Ge – Se)
	287.2	9.1	ν(Se – Se)
X	202.2	37.9	ν_{sym}(Ge – Se)
	283.3	9.4	ν(Se – Se)
XI	204.5	31.3	ν(Ge – Se)
	284.5	4.6	ν(Se – Se)
XII	190.9	33.8	ν(Ge – Se)
	201.7	15.6	ν(Ge – Se)
XIII	194.3	65.2	ν(Ge – Se)

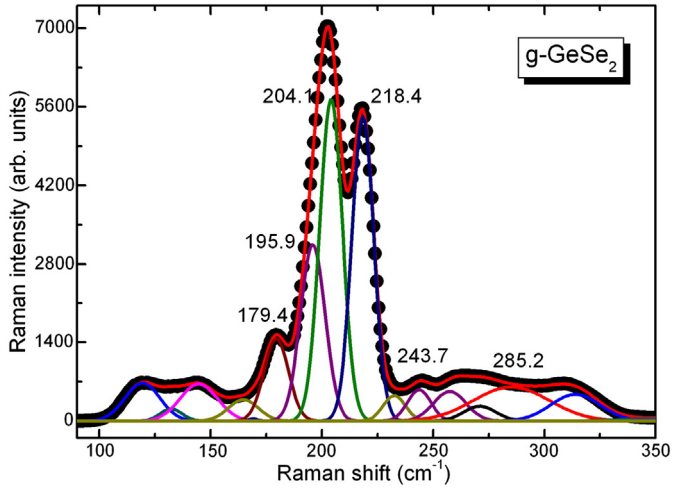

Fig. 4. High resolution micro-Raman spectra of *g*-$GeSe_2$ excited with the diode laser (785 nm) together with the results of curve fitting, performed by using Gaussian functions.

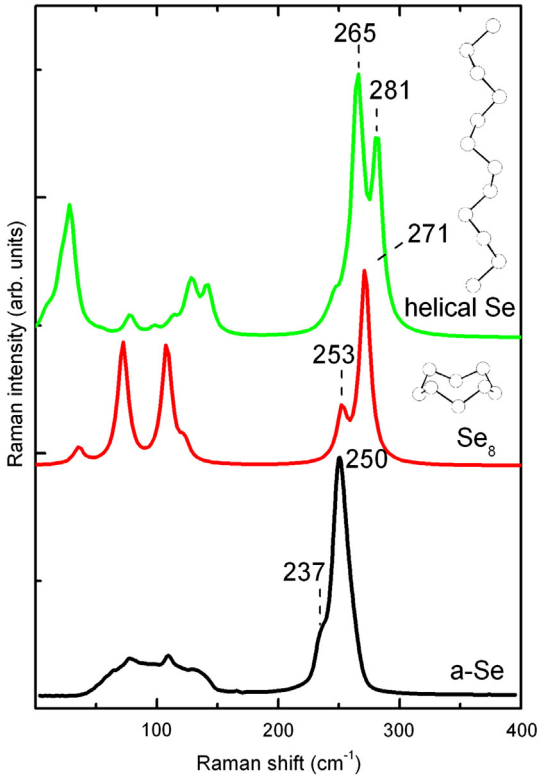

Fig. 5. Calculated Raman spectra of isolated Se_n (n = 12) chain and Se_8 ring (HSE06/LANL2DZ ECP polarized (p,d)) together with the experimental FT-Raman spectra of amorphous Se (*a*-Se) excited with near IR laser operating at 1064 nm.

4. Conclusions

The vibrational properties of Ge_nSe_m nanoclusters representing the short- and medium-range order structures of $GeSe_2$ crystal and "defect" clusters with homopolar Ge – Ge and Se – Se bonds that are thought to be related to the structural inhomogeneity found in $GeSe_2$ glass were studied in detail by using *ab initio* DFT method.

Detailed analysis of the experimental Raman spectra of *g*-$GeSe_2$ using curve fitting procedure showed the presence of nearly the same concentration of four- and six-member rings as well as bigger Ge–Se nanoclusters topologically similar with β-$GeSe_2$ crystal in the glass structure. Significant contributions of larger even-member rings ($i = 8, 10$) were detected.

Although five member rings with homopolar bonds were found to be energetically more favorable structures describing Ge – Ge and Se – Se bonds in *g*-$GeSe_2$ they cannot be unambiguously distinguished using the Raman spectroscopy due to similar frequency of Ge – Ge bond stretching vibrations and due to the broadening of the bands in the region of Se – Se stretching vibrations caused by asymmetric Ge – Se stretching vibrations.

A detailed study of the influence of synthesis condition and glass producing technology as well as laser induced transformation effects on population of different MRO structures in *g*-$GeSe_2$ are in progress.

Acknowledgments

This work was performed within Ukrainian–Turkish collaboration in Science and Technology (Project Numbers M85-2010 and TUBITAK-109T643).

References

[1] I. Fekeshgazi, K. May, V. Mitsa, A. Vakaruk, Physics and Applications of Non-crystalline Semiconductors in Optoelectronics, in: A. Andriesh, M. Bertolotti (Eds.), vol. 36, Kluwer Academic Publishers, Dordrecht/Boston/London, 1997, p. 243.
[2] In: M.F. Thorpe, L. Tichý (Eds.), Properties and Applications of Amorphous Materials, Proceedings of the NATO Advanced Study Institute, NATO Science Series II: Mathematics, Physics and Chemistry, Plenum/Kluwer, 2001.
[3] S.R. Ovshinsky, Phys. Rev. Lett. 21 (1968) 1450–1453.
[4] J.S. Sanghera, I.D. Aggarwal, L.B. Shaw, L.E. Busse, P. Thielen, V. Nguyen, P. Pureza, S. Bayya, F. Kung, J. Optoelectron. Adv. Mater. 3 (2001) 627–640.
[5] M.-L. Anne, J. Keirsse, V. Nazabal, K. Hyodo, S. Inoue, C. Boussard-Pledel, H. Lhermite, J. Charrier, K. Yanakata, O. Loreal, J. Le Person, F. Colas, C. Compère, B. Bureau, Sensors 9 (2009) 7398–7411.
[6] R. Holomb, V. Mitsa, O. Petrachenkov, M. Veres, A. Stronski, M. Vlček, Phys. Status Solidi C 8 (2011) 2705–2708.
[7] T. Ohta, J. Optoelectron. Adv. Mater. 3 (2001) 609–626.
[8] A. Zakery, S.R. Elliott, Optical nonlinearities in chalcogenide glasses and their applications, Springer Series in Optical Sciences, vol. 135, 2007.
[9] V. Ta'eed, N.J. Baker, L. Fu, K. Finsterbusch, M.R.E. Lamont, D.J. Moss, H.C. Nguyen, B.J. Eggleton, D.-Y. Choi, S. Madden, B. Luther-Davies, Opt. Express 15 (2007) 9205–9221.
[10] R.P. Wang, S.J. Madden, C.J. Zha, A.V. Rode, B. Luther-Davies, J. Appl. Phys. 100 (2006) 063524–063527.
[11] V. Mitsa, R. Holomb, M. Veres, A. Marton, I. Rosola, I. Fekeshgazi, M. Koós, Phys. Status Solidi C 8 (2011) 2696–2700.
[12] S.O. Kasap, K. Koughia, M. Munzar, D. Tonchev, D. Saitou, T. Aoki, J. Non-Cryst. Solids 353 (2007) 1364–1371.
[13] D.-Y. Choi, S. Maden, A. Rode, R. Wang, B. Luther-Davies, J. Non-Cryst. Solids 354 (2008) 3179–3183.
[14] J.S. Sanghera, C.M. Florea, L.B. Shaw, P. Pureza, V.Q. Nguyen, M. Bashkansky, Z. Dutton, I.D. Aggarwal, J. Non-Cryst. Solids 354 (2008) 462–467.
[15] M.M. Rahman, K. Rukmani, S. Asokan, J. Non-Cryst. Solids 357 (2011) 946–950.
[16] D. Reso, M. Silinskas, M. Lisker, E.P. Burte, J. Non-Cryst. Solids 358 (2012) 1511–1515.
[17] B.J. Eggleton, B. Luther-Davies, K. Richardson, Nat. Photonics 5 (2011) 141–148.
[18] S.R. Elliot, Physics of Amorphous Materials, Longman, New York, 1990.
[19] In: P. Boolchand (Ed.), Insulating and Semiconducting Glasses, World Scientific, Singapore, 2000.
[20] C. Quémard, F. Smektala, V. Couderc, A. Barthélémy, J. Lucas, J. Phys. Chem. Solid 62 (2001) 1435–1440.
[21] Q. Liu, X. Zhao, J. Non-Cryst. Solids 356 (2010) 2375–2377.
[22] R.T. Ananth Kumar, P. Chithra Lekha, B. Sundarakannan, D. Pathinettam Padiyan, Phil. Mag. 92 (2012) 1422–1434.
[23] K. Shimakawa, A. Kolobov, S.R. Elliott, Adv. Phys. 44 (1995) 475–588.
[24] K. Tanaka, J. Non-Cryst. Solids 352 (2006) 2580–2584.
[25] S. Sugai, Phys. Rev. Lett. 57 (1986) 456–459.
[26] V. Petkov, D. Le Messurier, J. Phys. Condens. Matter 22 (2010) 115402, (6 pp.).
[27] M. Kibalchenko, J.R. Yates, C. Massobrio, A. Pasquarello, J. Phys. Chem. C 115 (2011) 7755–7759.
[28] B.N. Ivanov-Emin, J. Gen. Chem. USSR 10 (1940) 1813–1818.
[29] G. Dittmar, H. Schäfer, Acta Crystallogr. B 32 (1976) 1188–1192.
[30] A.V. Novoselova, V.P. Zlomanov, S.G. Karbanov, O.V. Matveyev, A.M. Gas'kov, Prog. Solid State Chem. 7 (1972) 85–115.
[31] G. Dittmar, H. Schäfer, Acta Crystallogr. B 31 (1975) 2060–2064.
[32] G. Dittmar, H. Schäfer, Acta Crystallogr. B 32 (1976) 2726–2728.
[33] D.I. Bletskan, V.S. Gerasimenko, M.Yu. Sichka, Kristallografiya 24 (1979) 83–89, (in Russian).
[34] P.S. Salmon, I. Petri, J. Phys. Condens. Matter 15 (2003) S1509–S1528.
[35] P.S. Salmon, R.A. Martin, P.E. Mason, G.J. Cuello, Nature 435 (2005) 75–78.
[36] P.S. Salmon, J. Phys. Condens. Matter 19 (2007) 455208, (16 pp.).

[37] M. Cobb, D.A. Drabold, Phys. Rev. B 56 (1997) 3054–3065.
[38] M. Cobb, D.A. Drabold, R.L. Cappelletti, Phys. Rev. B 54 (1996) 12162–12171.
[39] C. Massobrio, A. Pasquarello, R. Car, Phys. Rev. B 64 (2001) 144205, (12 pp.).
[40] C. Massobrio, A. Pasquarello, Phys. Rev. B 77 (2008) 144207, (10 pp.).
[41] R. Holomb, V. Mitsa, S. Akyuz, E. Akalin, Phil. Mag. (2013), http://dx.doi.org/10.1080/14786435.2013.778426, (in press).
[42] D.I. Bletskan, N.M. Krolevec, M.Yu. Sichka, Phys. Technics Semicond. 10 (1976) 1817–1820, (in Russian).
[43] I.M. Migolinets, M.Yu. Sichka, Phys. Chem. Glas. 5 (1979) 287–290, (in Russian).
[44] R. Holomb, P. Johansson, V. Mitsa, I. Rosola, Phil. Mag. 85 (2005) 2947–2960.
[45] G. Lucovsky, R.J. Nemanich, F.L. Galeener, in: W.E. Spear (Ed.), Proceedings of the 7th International Conference on Amorphous and Liquid Semiconductors, CICL, Edinburgh, 1977, p. 125.
[46] P.M. Bridenbaugh, G.P. Espinosa, J.E. Griffiths, J.C. Phillips, J.P. Remeika, Phys. Rev. B 20 (1979) 4140–4144.
[47] H. Fjellvåg, K. Ove Kongshaug, S. Stølen, J. Chem. Soc. Dalton Trans. (2001) 1043.
[48] J.-E. Kwak, H. Yun, Acta Crystallogr. C 61 (2005) i81–i82.
[49] J.S. Sanghera, J. Heo, J.D. Mackenzie, J. Non-Cryst. Solids 101 (1988) 8–17.
[50] J.S. Sanghera, J. Heo, J.D. Mackenzie, R.M. Almeida, J. Non-Cryst. Solids 101 (1988) 18–22.
[51] B.E. Warren, J. Biscob, J. Am. Ceram. Soc. 21 (1938) 259–265.
[52] M.J. Frisch, G.W. Trucks, H.B. Schlegel, et al., Gaussian 03, Revision D.01, Gaussian, Inc., Wallingford CT, 2004.
[53] W. Kohn, L.J. Sham, Phys. Rev. 140 (1965) A1133–A1138.
[54] P.J. Hay, W.R. Wadt, J. Chem. Phys. 82 (1985) 284–298.
[55] C.E. Check, T.O. Faust, J.M. Bailey, B.J. Wright, T.M. Gilbert, L.S. Sunderlin, J. Phys. Chem. 105 (2001) 8111–8116.
[56] J. Heyd, G. Scuseria, J. Chem. Phys. 121 (2004) 1187–1192.
[57] J. Heyd, G.E. Scuseria, M. Ernzerhof, J. Chem. Phys. 124 (2006) 219906.
[58] R. Holomb, V. Mitsa, Solid State Commun. 129 (2004) 655–659.
[59] T.G. Edwards, S. Sen, E.L. Gjersing, J. Non-Cryst. Solids 358 (2012) 609–614.
[60] S. Sugai, Phys. Rev. B 35 (1987) 1345–1361.
[61] T.G. Edwards, S. Sen, J. Phys. Chem. B 115 (2011) 4307–4314.
[62] L.F. Santos, A. Ganjoo, H. Jain, R.M. Almeida, J. Non-Cryst. Solids 355 (2009) 1984–1988.
[63] R.J. Nemanich, S.A. Solin, G. Lucovsky, Solid State Commun. 21 (1977) 273–276.
[64] Y. Wang, K. Tanaka, T. Nakaoka, K. Murase, Phys. B 316&317 (2002) 568–571.
[65] P. Boolchand, P. Chen, M. Jin, B. Goodman, W.J. Bresser, Phys. B 389 (2007) 18–28.
[66] P. Boolchand, W.J. Bresser, Phil. Mag. B 80 (2000) 1757–1772.
[67] J.E. Griffiths, G.P. Espinosa, J.P. Remeika, J.C. Phillips, Solid State Commun. 40 (1981) 1077–1080.
[68] J.E. Griffiths, G.P. Espinosa, J.P. Remeika, J.C. Phillips, Phys. Rev. B 25 (1982) 1272–1286.
[69] T. Nakaoka, Y. Wang, K. Murase, Phys. Rev. B 63 (2001) 224206, (5 pp.).
[70] G. Lucovsky, C.K. Wong, W.B. Pollard, J. Non-Cryst. Solids 59&60 (1983) 839–846.
[71] R.J. Nemanich, F.L. Galeener, J.C. Mikkelsen Jr., G.A.N. Connel, G. Etherington, A.C. Wright, R.N. Sinclair, Phys. B 117&118 (1983) 959–961.
[72] K. Jackson, A. Briley, S. Grossman, D.V. Porezag, M.R. Pederson, Phys. Rev. B 60 (1999) R14985–R14989.
[73] P. Boolchand, X. Feng, W.J. Bresser, J. Non-Cryst. Solids 293–295 (2001) 348–356.
[74] V.V. Poborchii, A.V. Kolobov, J. Caro, V.V. Zhuravlev, K. Tanaka, Chem. Phys. Lett. 280 (1997) 17–23.
[75] V.V. Poborchii, A.V. Kolobov, J. Caro, V.V. Zhuravlev, K. Tanaka, Phys. Rev. Lett. 82 (1999) 1955–1958.